Turbulence observations of the nearshore wave bottom boundary layer

D. L. Foster,[1] R. A. Beach,[2] and R. A. Holman[3]

Received 25 January 2005; revised 24 October 2005; accepted 13 January 2006; published 27 April 2006.

[1] Field observations of turbulence and sediment suspension in the nearshore wave bottom boundary layer obtained during the Duck94 field experiment on the North Carolina coast showed the generation of near-bed turbulence to be highly intermittent. The intermittent nature of the flow was examined by applying homogeneous isotropic turbulence laws over small windows of data. The time-varying estimates of turbulent kinetic energy, shear stress, dissipation, and concentration were averaged over the phase of the free stream wave. The observations show that the magnitude of the turbulent kinetic energy is largest under the wave crest and decreases over the decelerating flow phase until reversal to offshore flow. The turbulent kinetic energy observations under the crests compare favorably to those of three laboratory studies. The sediment suspension observations were shown to have an intermittent structure and to be biased toward the onshore decelerating phase of the flow. The shear stress was estimated with the orbital velocities by assuming an eddy viscosity model and was shown to be highly sensitive to the free stream velocity and less sensitive to the free acceleration. The intermittent signal of the turbulent kinetic energy and the suspension was not evident in the shear stress estimates, providing further support that eddy viscosity models are not appropriate for predicting the suspension of sediment. Finally, dissipation rate estimates increased with proximity to the bed but were several orders of magnitude lower than those found in the active breaking region.

Citation: Foster, D. L., R. A. Beach, and R. A. Holman (2006), Turbulence observations of the nearshore wave bottom boundary layer, *J. Geophys. Res.*, *111*, C04011, doi:10.1029/2004JC002838.

1. Introduction

[2] Energetics-based sediment transport models assume the transport of suspended sediment is proportional to the time averaged energy dissipation of the fluid on the bottom [*Bagnold*, 1966; *Bowen*, 1980; *Bailard*, 1981]

$$i_s \propto |u\tau_b|, \tag{1}$$

where i_s is the immersed weight transport of suspended sediment, u is the total cross-shore velocity, and τ_b is the bed stress. Because the actual bed stress is unknown, these models often rely on simple quadratic or eddy viscosity parameterizations. An intrinsic assumption with these models is that the generation of turbulence is solely due to the bottom stress that leads to the prediction that the transport of suspended sediment is proportional to the strength of and will oscillate with the wave velocity. Suspended sediment field observations show an increase in concentration with increasing wave strength; however, the concentration spikes are intermittent and not simply proportional to the oscillating wave velocities [*Jaffe et al.*, 1984; *Huntley and Hanes*, 1987; *Hanes*, 1988; *Beach and Sternberg*, 1992; *Smyth and Hay*, 2003]. These observations suggest that suspension events are a result of rapid aperiodic turbulence introduction to the near-bed region. The generation of these turbulence events may have its source at the bottom because of bottom shear, within the wave bottom boundary layer because of to shear instabilities, and/or near the free surface because of downward advected surface wave breaking.

[3] In a wave-dominated environment, the boundary layer is under continual development because of the oscillatory nature of the velocity, and its size is limited by the magnitude and period of the waves. The velocity oscillations and resulting shear create an unsteady generation of turbulence. Under periods of increasing generation, we expect to see a steeper slope in the velocity wave number spectrum because energy is being input faster than it is dissipated. However, under periods of decreasing generation, we expect to see flatter slopes because energy is being dissipated faster than it is being generated.

[4] A laboratory investigation of oscillatory flow over a smooth bed found that turbulence generation rates are

[1]Department of Civil and Environmental Engineering and Geodetic Science, Ohio State University, Columbus, Ohio, USA.
[2]Consortium for Oceanographic Research and Education, Washington, D. C., USA.
[3]College of Oceanic and Atmospheric Sciences, Oregon State University, Corvallis, Oregon, USA.

0148-0227/06/2004JC002838$09.00

highest at the beginning of flow deceleration (decreasing velocity magnitude) and that this energy is completely dissipated within the deceleration period [*Hino et al.*, 1983]. A later study of flow over a rough bed found that turbulent intensities are greatest during the flow deceleration period and in phase with the Reynolds Stress [*Sleath*, 1987]. The investigation also showed that during the acceleration (increasing velocity magnitude) phase of the flow, the frequency spectral energy slope followed a Kolmogorov $-5/3$ spectrum, but during the deceleration phase of the flow, the spectrum slope was significantly steeper. Under rough bed oscillatory boundary layers, the near-bed turbulent intensities and Reynolds stresses have been found to be 50% higher than for a smooth bed [*Jensen et al.*, 1989].

[5] The first field investigation of the development of turbulence in a wave bottom boundary layer (WBBL), paired visual observations with a hot film anemometer concluded that the flow in a fluid-granular boundary layer undergoes a transition from laminar to turbulent only under wave crests [*Conley and Inman*, 1992]. An Oregon coast wave bottom boundary layer investigation concluded that suspension events were well correlated with high-frequency ($f > 8$ Hz) velocity variance events and that some of those events could have been triggered by a shear instability within the wave bottom boundary layer [*Foster et al.*, 1994]. More recently, field observations of vertical velocity over a variety of bed states were used to examine the turbulent properties within the wave bottom boundary layer [*Smyth and Hay*, 2003]. The observations showed evidence of anisotropy with a flattening of the spectral slope as the bed was approached. The variable bed roughness provided by the 4 bed states resulted in turbulent intensities with similar magnitudes.

[6] The first quantitative field observations of surf zone turbulence levels found that dissipation rates to vary from 4 $cm^2\ s^{-3}$ in the lower water column to 200 $cm^2\ s^{-3}$ at the surface (assuming a 2 m water depth) [*George et al.*, 1994]. Estimates of dissipation rates made with the observations compared well to the bore dissipation model of *Thornton and Guza* [1983]. The estimates of dissipation rates were significantly lower than those predicted by lab studies and decrease with decreasing sensor elevation (although a slight increase was found at the lowermost position). If turbulence is being generated at the bed, it is conceivable that larger dissipation estimates will be found in the wave bottom boundary layer than in the lower water column.

[7] The observations presented here are used to examine the temporal and vertical variations of bottom boundary layer dynamics and energetics with simultaneous sediment suspension measurements. A vertical array of four hot film anemometers are colocated with a vertical stack of 20 fiber optic back scatter sensors (FOBS). The unique nature of these measurements allow us to examine the interaction between waves, turbulence and sediment suspension in the surf zone.

[8] Using data collected during the Duck94 field experiment, we examine the evolution of the turbulent kinetic energy and sediment suspension of the wave phase. The observations are compared with the evolution of the shear stress estimated with the orbital wave velocities assuming an eddy viscosity closure model. The field observations are summarized in section 2, the results are presented in section 3, and conclusions are given in section 4.

2. Observations

[9] The measurements were collected at the Army Corps of Engineers Field Research Facility in Duck, North Carolina on 17 August 1994 as part of the Duck94 cooperative field experiment. The offshore Significant wave height, peak wave period, and dominant incoming angle of the peak wave period as measured at the 8 m array were 0.83 m, 4.5 s, and 50° from the southeast, respectively. The barred beach was composed of well-sorted fine-grained sand ($D_{50} = 0.2$ mm). The observations were made in 2 m water depth on the seaward side of the bar crest under mostly unbroken waves. Theoretical estimates of the wave bottom boundary layer thickness varied from 2.2 to 4.0 cm [*Foster et al.*, 2000].

[10] Velocity and speed measurements used in this investigation were made with four TSI model 1755 constant temperature cylindrical quartz coated hot film anemometer probes stacked with a 1 cm vertical spacing, and one Marsh-McBirney electromagnetic current meter. The dominant hot film signal is a measure of the cross shore velocity magnitude, and, as used in this investigation, has a frequency response of 128 Hz. The calibrated velocity magnitude of each hot film signal was derectified by searching for local minima around windows of the free streamflow reversal. Sediment suspension was measured at a 16 Hz sampling rate with a 19 sensor fiber-optic back scatter (FOBS) probe. In addition to measuring the sediment suspended in the water column, the FOBS also pierces the bed and measures bed elevation as sensors are alternatively covered and uncovered. The presence of bed forms was determined visually with an underwater video camera. The instruments were deployed from a cantilevered arm attached to the boom of a crane (hereinafter referred to as SIS) located on the FRF pier. To prevent vibration, a spike attached to the end of the boom was set into the bed and held in place by the weight of the crane. The vibration of the SIS was measured with an accelerometer located near the spike on the lower boom. The exact orientation of the accelerometer was unknown, so the orthogonal coordinated axis was rotated to align the downward acceleration with gravity. The accelerometer observations were contaminated by an unknown aliased signal that resulted in energy that was uncorrelated to any wave or mean flows present. This signal was partially removed with a band pass filter. The reader is referred to *Foster et al.* [2000] for a complete review of the instrumentation capabilities, deployment, and calibration.

[11] Over the course of the 10 min calibration record and 34 min WBBL record, the bed underwent both erosion and accretion, causing the hot film array's relative elevation from the bed to vary. We will focus on seven independent 256 s records, which include (1) five records within the lowest 5 cm of the water column where the hot film gain and the bed elevation remained uniform (runs 1–5) and (2) two records from the 10 min calibration run (runs 6–7), where the sensor elevations

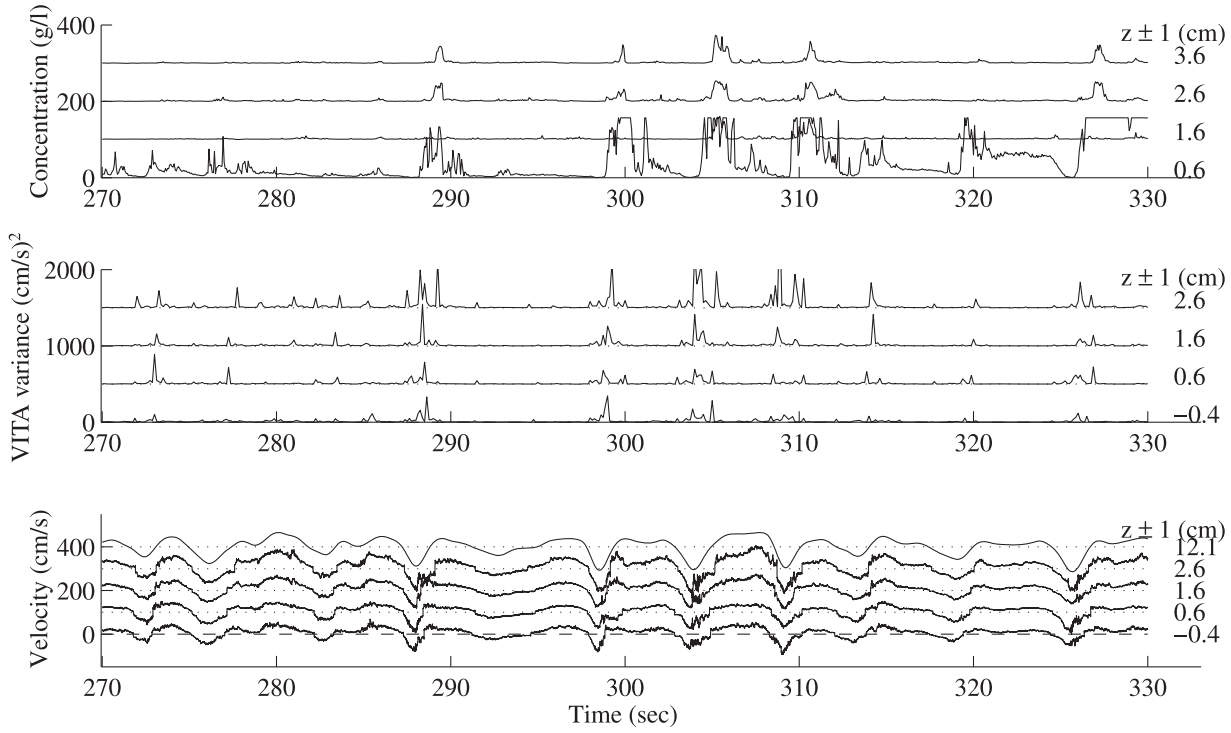

Figure 1. (bottom) Example 60 s time series near-bed cross-shore velocity as measured by four hot film anemometers and the free stream velocity as measured by the Marsh-McBirney electromagnetic current meter; (middle) high-frequency variable interval time average velocity variance at four elevations above the bed; and (top) concentration at four elevations above the bed. The average distance of each sensor from the bed as measured by the FOBS over the 60 s record is listed on the right. Each velocity, variance, and concentration time series is offset by 100 cm s^{-1}, 500 (cm s^{-1})^2, and 100 g L^{-1}, respectively. Onshore-directed flow is defined with negative velocities, and offshore-directed flow is defined with positive velocities.

were outside the wave bottom boundary layer and varied from 13–17 cm above the bed [*Foster*, 1996].

[12] Figure 1 shows an example 60 s time series of cross-shore velocity, high-frequency velocity variance, and sediment concentration at several elevations above the bed. Throughout this paper it is assumed that onshore-directed flow is negative and offshore-directed flow is positive. Characteristic of theoretical boundary layers, the velocity magnitude decrease with sensor proximity to the bed (Figure 1). The high-frequency velocity variance, a measure of the localized turbulent energy, is determined with the variable interval time average (VITA) technique, defined with [*Blackwelder and Kaplan*, 1976]

$$\widehat{var}(z,t) = \frac{1}{T}\int_{t-\frac{T}{2}}^{t+\frac{T}{2}} u^2(z,s)ds - \left(\frac{1}{T}\int_{t-\frac{T}{2}}^{t+\frac{T}{2}} u(z,s)ds\right)^2, \qquad (2)$$

where T is the window size (1/16 s for Figure 1), u is the total velocity at each elevation, z is the elevation from the bed and t is time. This window size was selected because it is the timescale over that significant sediment response is observed with the FOBS. The size of the window primarily effects the magnitude of turbulence events, and not the presence or absence of events. For bottom generated turbulence, the VITA variance should increase with increasing elevation within the WBBL and decrease outside the WBBL. In agreement with an Oregon coast investigation of *Foster et al.* [1994], intermittent concentration observations are coherent with intermittent high-frequency velocity variance structure. Visual inspection shows that several of these events are paired with the larger wave events.

[13] The power spectral density of the individual sensors within an array showed decreasing variance with increasing proximity to the bed [*Foster et al.*, 2000]. The spectra also show a slope break at approximately 1 Hz that is indicative of a change between the dominance of wave to turbulent motions. Figure 2 shows the frequency spectra (calculated as specified by *Priestley* [1981] for the uppermost hot film sensor in the 6 runs. Next to each of the offset frequency spectra is an estimate of the vertical SIS vibration velocity and displacement. Approximates of the SIS frame velocity and displacement were determined by integrating an accelerometer signal once and twice, respectively. In all cases the RMS frame velocity and displacement was less than 1.4 cm s^{-1} and 0.3 cm. The energy spike at 50 Hz present in the calibration run 6 was a result of sting vibrations.

[14] The total velocity is partitioned into wave and turbulent motions with

$$u = \tilde{u} + u', \qquad (3)$$

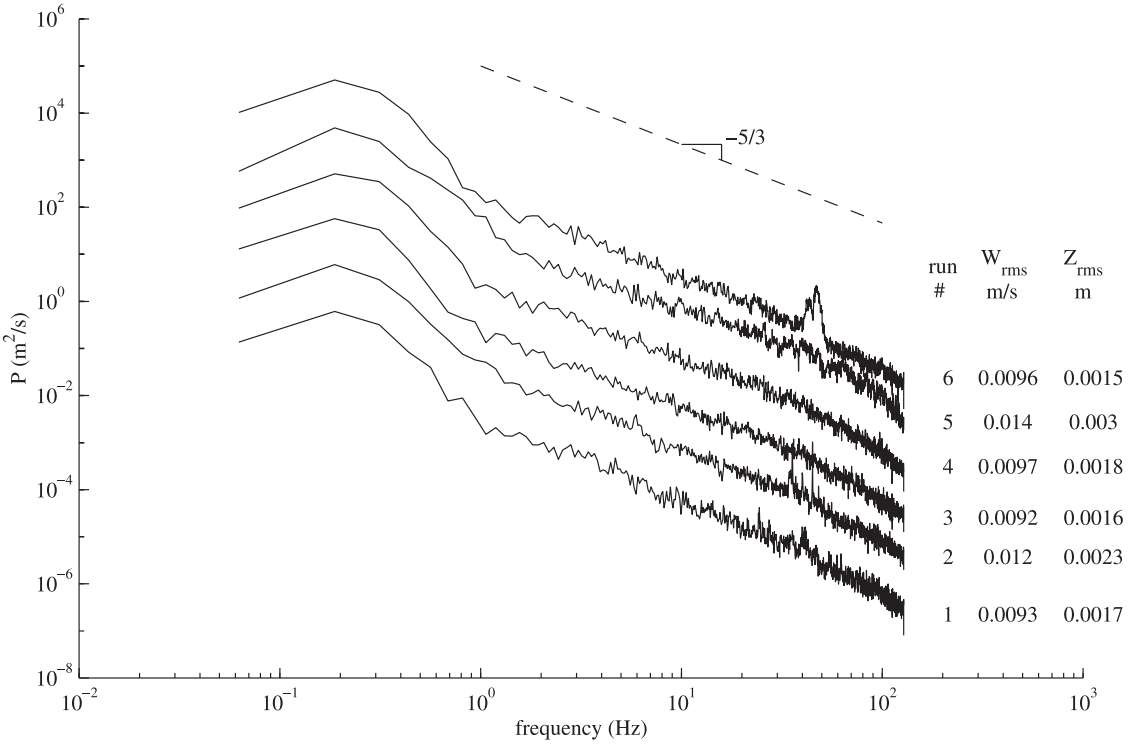

Figure 2. Energy density spectra as a function of the frequency for runs 1–6 for the uppermost sensor in the array. Each spectrum is offset one decade. Right-hand columns adjacent to each spectrum show the RMS velocity and displacement for the frame. The one-sided power spectral density of each independent 256 s time series was calculated with eight ensemble averages and four frequency band averages, leading to 64 degrees of freedom. Each ensemble average was demeaned, detrended, and modified by a variance conserving Hanning window.

where $\tilde{u}$ is assumed to be the wave and mean flow motions partitioned to frequencies less than 2 Hz and u' is assumed to be the turbulent motions partitioned to frequencies greater than 2 Hz. Because it is not possible to identify a specific frequency or wave number break between wave and turbulent motions, we separate low-frequency wave and current motions from turbulence motions at 2 Hz that is beyond the 1 Hz slope break. This frequency cutoff excludes the turbulent energy at the lowest turbulent frequencies; however, it also decreases the likelihood of leaking wave motions to the following turbulence analysis. A sensitivity analysis to the length of the sampling window (ranging from 1/2 s to 1/16 s) showed only a variation in magnitude and not the absence or presence of events. The turbulent variance predicted with this method will be lower than the true turbulent variance.

3. Results

[15] The wave and turbulent velocities are determined by defining wave motions to be the mean value over 1/2 s windows at consecutive 1/16 s overlapping steps,

$$\tilde{u}(t_n) = \frac{1}{T_2} \sum_{n-\frac{t_2}{2}+1}^{n-\frac{t_2}{2}} u(t_n)\Delta t, \tag{4}$$

where T_2 is 1/2 s window. The 1/2 s was specified to be consistent with the 2 Hz cutoff frequency. In a manner consistent with *George et al.* [1994], a considerably smaller 1/16 s overlap resulted in 4096 estimates for a single 256 s window. The remaining variance determined with (3) is defined herein as turbulence.

[16] The majority of turbulence investigations have been conducted in laboratories under sinusoidal waves. Consequently, it has been convenient to present the results as a function of wave phase (i.e., 0° to 360°). Because waves in the surf zone are random, we define an analogous random wave phase as a function of the instantaneous free stream velocity and acceleration. This phase space averaging (PSA) technique allows for the evaluation of the magnitude and evolution of physical quantities, such as suspended sediment concentration, turbulent kinetic energy, and dissipation over the wave phase space. Each quantity of interest (for each 256 s data segment) is averaged over concurrently measured free stream velocity, $\tilde{u}_\infty$, and free stream acceleration, $d\tilde{u}_\infty/dt$ bins. The seven free stream velocity bins for each of the seven runs are centered on −140, −100, −60, −20, 20, 60, 100 cm s^{-1} with a ±20 cm s^{-1} window about each bin. Similarly, the six free stream acceleration bins are centered on −250, −150, −50, 50, 100, 150, 250 cm s^2 with a ±50 cm s^2 window about each bin. The free stream acceleration is determined in the frequency domain with a 1 Hz low-pass cutoff frequency and is defined with

$$\frac{d\tilde{u}_\infty}{dt} = \frac{1}{2\pi} \int_{-f_{cut}}^{f_{cut}} \imath 2\pi s \left[\int_{-\infty}^{\infty} \tilde{u}_\infty(\tau) e^{-\imath t s} d\tau \right] e^{-\imath t s} ds, \tag{5}$$

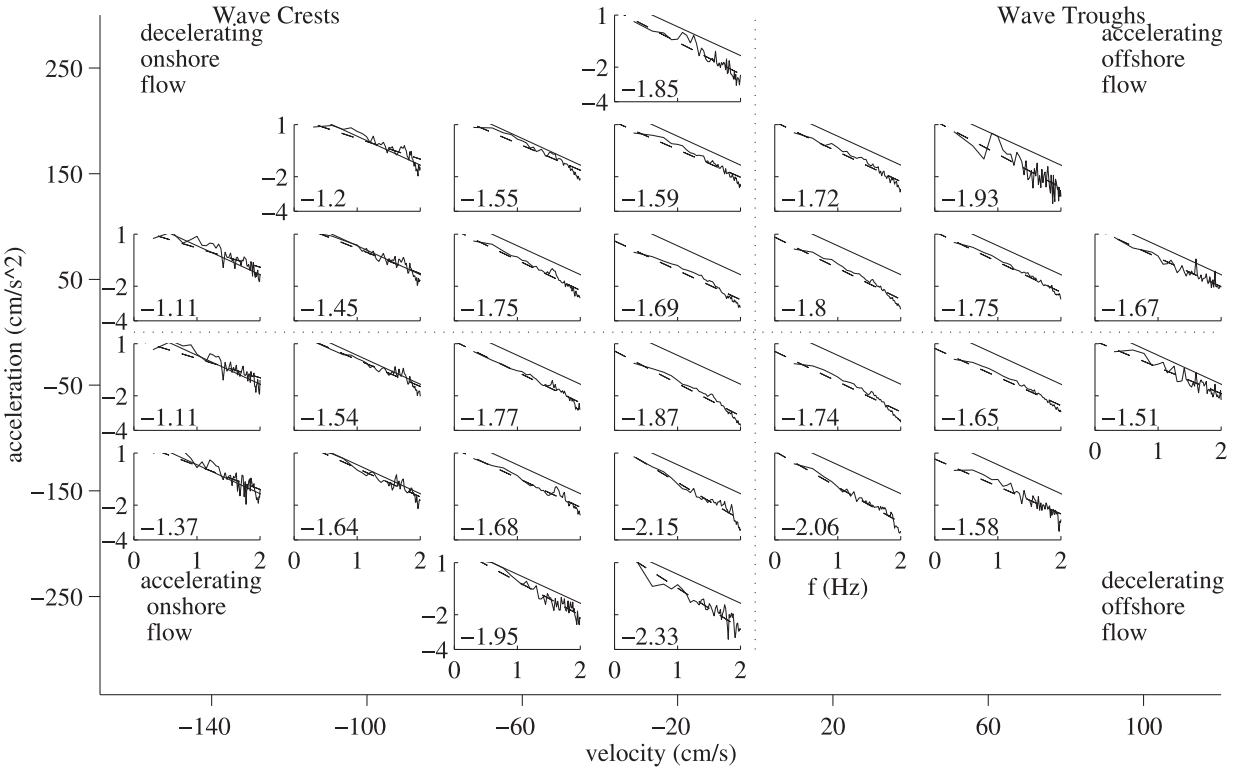

Figure 3. Phase space average distribution of velocity energy density spectrum at 4 cm above the bed versus frequency during one 256 s record. The vertical axis of each independent plot is energy density ((cm s^{-1})^2 Hz^{-1}), and the horizontal axis is frequency, ranging from 1 to 100 Hz. The spectra were calculated over 1/2 s windows of data with a 1/16 s overlap. The slope of each spectrum is given in the lower-left hand corner of each plot.

where f_{cut} = 1 Hz. The sample mean of the quantity in each bin is computed, producing a "phase space" average. If the waves were purely sinusoidal with a single amplitude, the PSA would lead to an ellipse with a vertical (acceleration) to horizontal (velocity) ratio of ω. For minimal statistical stability, we require that at least three realizations be present in each observation. The flow moves in a clockwise direction around each of the following figures. Because the free stream velocity and acceleration are different for each of the 5 (sometimes 7) segments, not all phases will contain the same number of estimates. In describing the following results, we define acceleration as the derivative of the velocity (5), but the phrase "accelerating flow" indicates flow that has an increasing velocity magnitude and similarly "decelerating flow" indicates flow that has a decreasing velocity magnitude.

3.1. Turbulent Kinetic Energy

[17] Energy density frequency spectra were calculated by prewhitening each 1/2 s window of velocity with a first difference filter and then post coloring in the frequency domain by removing the effect of the high-pass time domain filter [*Priestley*, 1981]. This method proved to be the most robust method for eliminating the leakage of the dominant low-frequency signal. Example PSA spectra for a single 256 s velocity record at 4 cm above the bed is shown in Figure 3. A line was fit to the observations with a weighted (log(f)) least squares analysis, over the frequency range of 2 to 100 Hz, at each phase. The upper frequency of 100 Hz was limited by the instrument resolution. Because it is not possible to show all the PSA spectra distributions from each sensor and each run, we approximate all spectra with each turbulent slope and integrated variance (Figures 4 and 5).

[18] There exists a trend in the slopes from flatter than $-5/3$ to steeper than $-5/3$ as velocity magnitudes decrease from peak values to zero velocity. This trend is present in all seven runs. The flatter slopes are present under the peak velocities for both crests and troughs. Steeper slopes are present during the velocity zero crossings. Because the universal equilibrium theory of turbulence predicts $-5/3$ slopes of wave number spectra and not wave frequency spectra, this last observation may be an effect of the low and potentially variable advective velocity ($\tilde{u}$). The criteria needed to transform from frequency to wave number space is discussed in section 3.4.

[19] The integrated variance (turbulent kinetic energy (TKE)) is defined as the integral of the energy frequency spectra (F(f)) from 2 to100 Hz. As before noted, we recognize that turbulent motions that have frequencies lower than 2 Hz will be excluded and consequently the values reported here are expected to be lower than the true TKE magnitudes, Figure 5. Under mild wave conditions ($|u| <$ 80 cm s^{-1} and $|u_t| < 200$ cm s^2), the turbulent kinetic energy increases approximately linearly with elevation from the bed until outside the WBBL where energy magnitudes in the free stream are generally lower than those in the upper elevations within the WBBL. This situation is characteristic

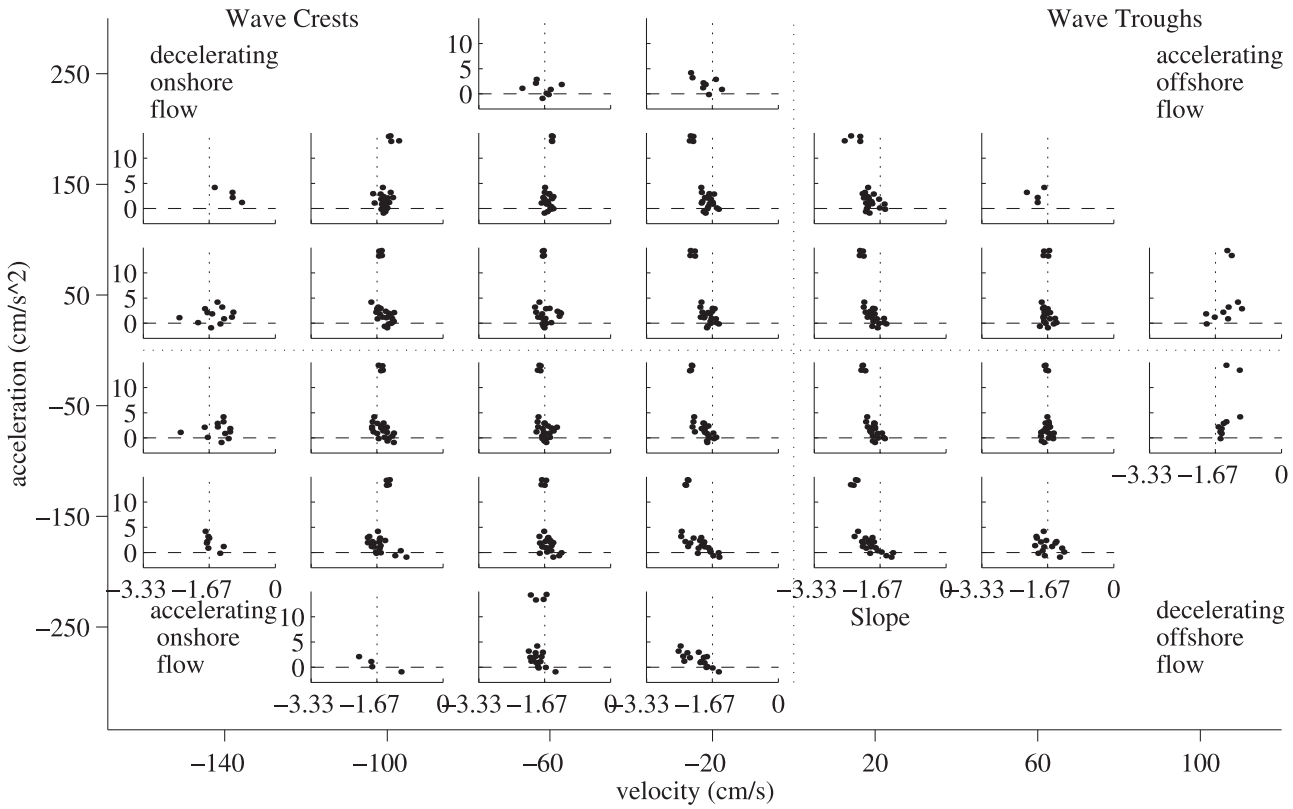

Figure 4. Phase space average distribution of frequency slopes versus the sensor elevation of the five 256 s WBBL segments. The vertical axis of each independent plot is elevation from the bed, ranging from −2 to 15 cm, and the horizontal axis is slope, ranging from −10/3 to 0.

of the bottom shear generated turbulence that scales with elevation away from the bed within the WBBL. Turbulence levels begin to increase following the transition from offshore to onshore flow. Under the large crests ($\tilde{u}_\infty < -80$ cm s^{-1}), turbulence levels are significantly larger and more variable, than in most other wave phases.

[20] The TKE is largest under the wave crest and decreases over the decelerating flow until reversal to offshore flow. In agreement with *Hino et al.* [1983] and *Sleath* [1987], the turbulent kinetic energy has significantly decreased by the time of flow reversal. These observation show that the enhanced turbulent kinetic energy levels are achieved during the latter stages of the onshore accelerating flow. Hino et al. and Sleath also observed an increasing horizontal turbulent intensity at the latter stages of the accelerating flow, and Hino et al. further concluded that the turbulence was suppressed until the flow begins its decelerating phase. These observations show only mildly enhanced turbulent kinetic energy levels under the troughs for comparable velocity magnitudes to those under the crests. The lower energy levels may be indicative of a sensitivity of turbulence generation to acceleration magnitudes as well as velocity magnitudes or possible wave breaking inshore of the array. According to video observations, only occasional waves were actively breaking near the instrument frame. Possible influence due to wave breaking may be evident in the elevated TKE amplitudes outside the boundary layer for the extreme wave crests ($U_\infty < 100$ cm s^{-1}). An additional and equally plausible explanation is that the increased suspended sediment concentrations under the wave troughs dampen the turbulence. Unfortunately, the purely sinusoidal laboratory wave velocities leave us without comparison in attempting to explain the discrepancies between the wave crest and troughs.

3.2. Suspended Sediment Concentration

[21] The PSA technique is performed on five concentration sensors with elevations ranging from 0 to 13 cm above the bed and over the five 256 s segments, Figure 6. The individual subplots show a noticeable break in the log concentration slope at 5–7 cm above the bed and are of order the wave bottom boundary layer thickness. The extremely high PSA concentration near the bed are likely sensors that are fluctuating about the bed level. The high fluid-sediment interface concentration levels (at the bed-water interface), primarily occur in all quadrants of the flow except during the onshore accelerating flow. Other than the near-bed sensors, the suspension is largest following the wave crest as the flow transitions from onshore to offshore. The sediment plumes present during the accelerating offshore flow generally lag the large amplitude TKE plumes by 1/2 s. An analysis of plume displacement showed that the plumes present during the decelerating onshore flow are the same as those present during the accelerating offshore flow.

3.3. Shear Stress

[22] In (1) the transport of suspended sediment is assumed to be proportional to the shear stress, τ. Because it is not possible to solve for the Reynolds stress directly, it is

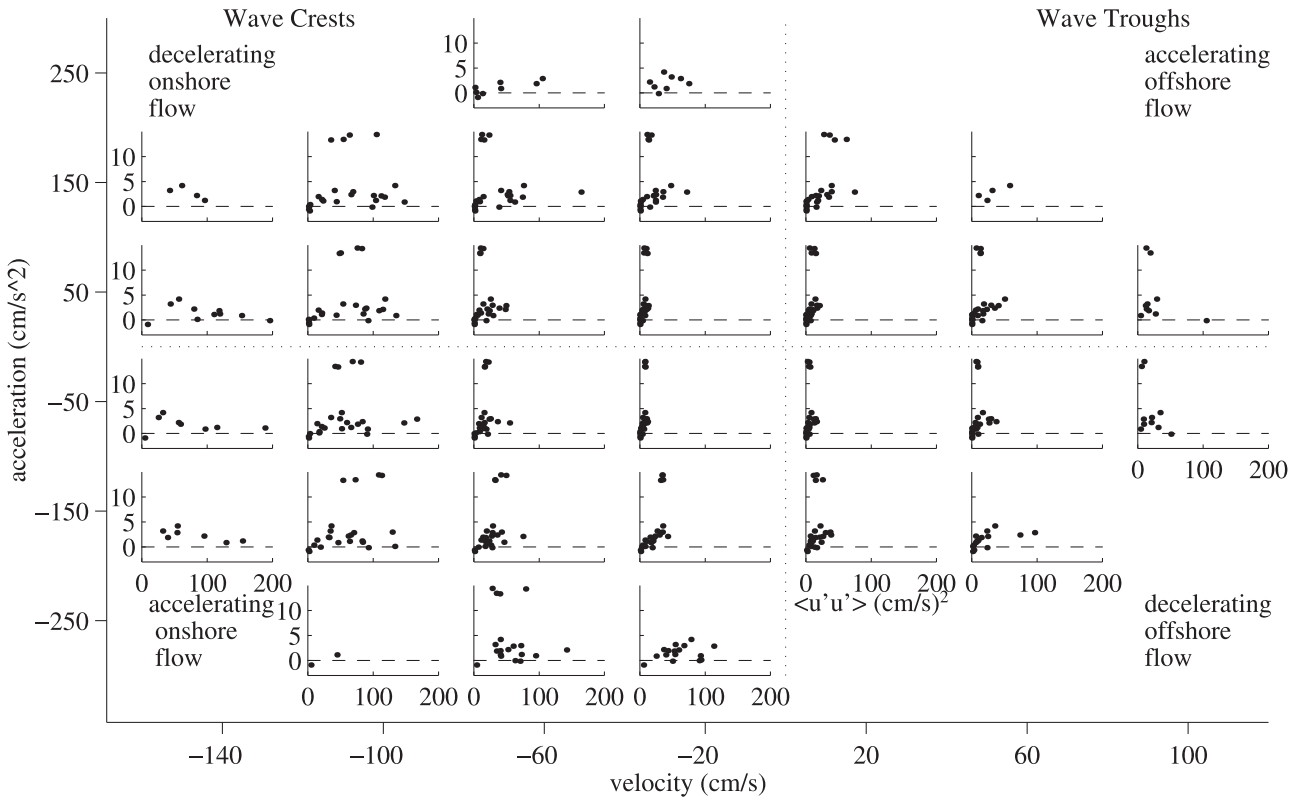

Figure 5. Phase space average distribution of turbulent kinetic energy versus the sensor elevation of the five 256 s WBBL segments. The vertical axis of each independent plot is elevation from the bed, ranging from −2 to 15 cm, and the horizontal axis is stress, ranging from 0 to 200 (cm s^{-1})^2.

commonly approximated with a zero equation turbulence closure eddy viscosity model

$$\frac{\tau}{\rho} = -\overline{u'w'} \approx \nu_t \frac{\partial \tilde{u}}{\partial z}, \tag{6}$$

where τ is the stress, and ν_t is the eddy viscosity model. The velocity gradient, $\frac{\partial \tilde{u}}{\partial z}$, is approximated numerically as $\frac{\Delta \tilde{u}}{\Delta z}$ with the hot film array and by assuming the velocity at the bed to be zero. The eddy viscosity is defined here with

$$\nu_t \equiv \kappa u_* z, \tag{7}$$

where κ is Von Karman's constant (=0.41) and $u_*(\equiv\sqrt{\tau_o/\rho})$ is the bed shear velocity. The bed shear velocity is estimated here with

$$u_* = \kappa z_o \left[\frac{\partial \tilde{u}}{\partial z}\right]_{z=z_o}, \tag{8}$$

where z_o is the bed roughness. Previous estimates of the bed shear velocity have been made by fitting logarithmic and exponentially decaying models to the RMS velocity observations. Here, an estimate of the bed shear velocity is required at each instant in time. Because the above models are not appropriate during velocity zero crossings, the bed shear velocity is calculated by assuming that u_* may be represented with

$$\frac{\partial \tilde{u}(z_o,t)}{\partial z} \approx \alpha \tilde{u}(z_o,t) + \beta \tilde{u}(z_o+z_1,t) + \gamma \tilde{u}(z_o+z_2,t), \tag{9}$$

where α, β, and γ are unknown constants and z_1 and z_2 are elevations of the two closest near-bed velocity sensors. A Taylor series expansion is performed on each term in (9) and truncated to 3 terms, similar terms are collected, and coefficients (α, β, and γ) are determined [*Foster*, 1996]. If the velocity at the bed is assumed to be zero, then the bed shear estimate becomes

$$\frac{\partial \tilde{u}(z_o,t)}{\partial z} \approx -\frac{z_2}{z_1(z_1-z_2)}\tilde{u}(z_o+z_1,t) + \frac{z_2}{z_1(z_1-z_2)}\tilde{u}(z_o+z_2,t). \tag{10}$$

Once the bed shear velocity is estimated, the shear stress is estimated with (6). Figure 7 shows the shear stress for the five segments of data at the four hot film elevations. At nearly all phases of the flow the shear increases linearly from the bed. The linear shear stress is indicative of uniform velocity shear through the water column ($\frac{\partial \tilde{u}}{\partial z}$ = constant) and is not in disagreement with laboratory and theoretical studies that showed the Reynold stress increasing to some elevation within the boundary layer before decreasing [*Hino*

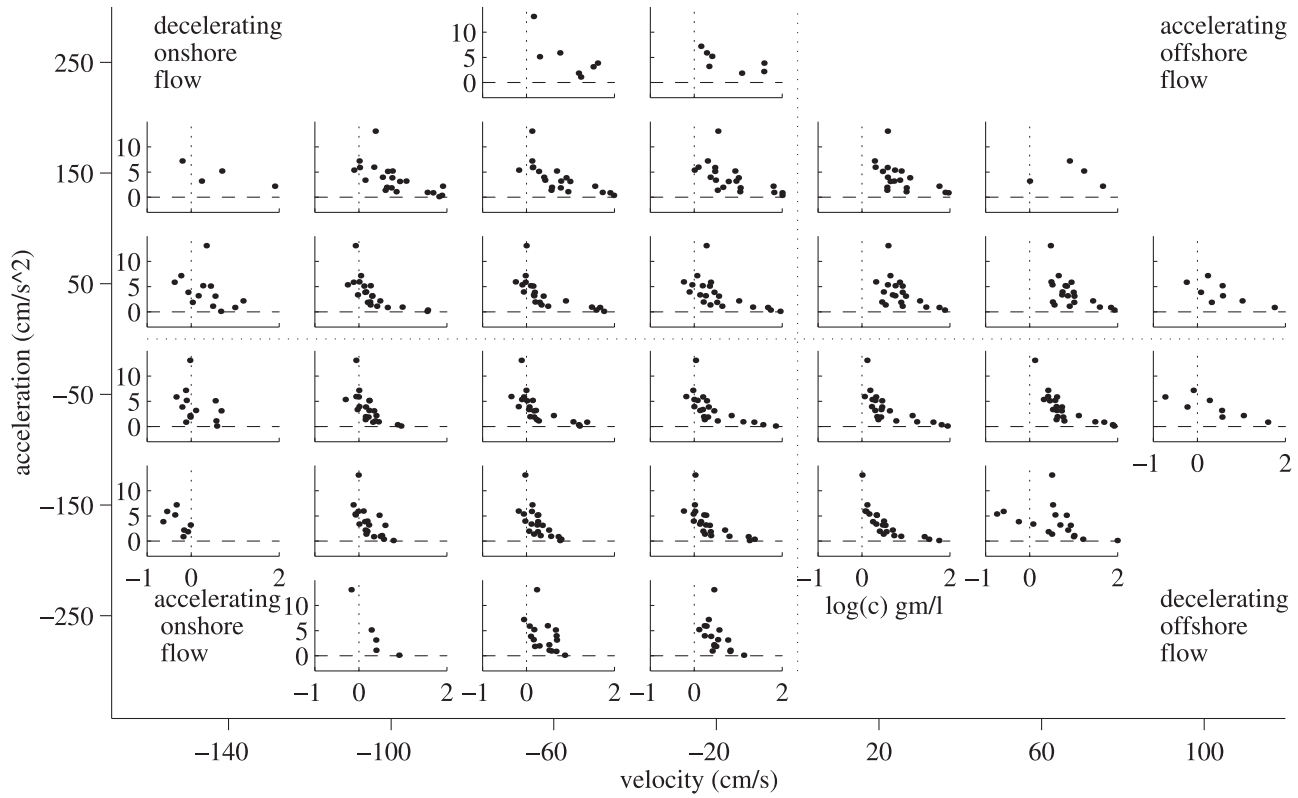

Figure 6. Phase space average distribution of the log concentration versus the sensor elevation of the five 256 s WBBL segments. The vertical axis of each independent plot is elevation from the bed, ranging from −2 to 15 cm, and the horizontal axis is concentration, ranging from 0 to 100 g L^{-1}. Each phase space average was required to have at least three realizations in each bin to be included.

et al., 1983; *Jensen et al.*, 1989]. The largest shear stress is present under the crests and troughs of the waves. However, the stress is larger under the troughs than under the crests for the same velocity magnitudes (see the ±100 cm s^{-1} bins). This is likely attributed to the longer excursion time of the troughs, which allow the boundary layer to develop more fully than under the shorter duration crests. The estimated shear stress is relatively insensitive to free stream acceleration and is highly sensitive to the free stream velocity. The oscillatory nature of the estimated shear stress does not agree favorably with the PSA concentration structure that is biased toward the positive accelerations following the wave crests.

3.4. Dissipation Rate

[23] Dissipation was calculated by following the technique of *George et al.* [1994]. In homogeneous isotropic turbulence, the universal form of the velocity spectra over the inertial subrange is defined with

$$\Phi(k) = \alpha\epsilon^{2/3}k^{-5/3}, \tag{11}$$

where α is a nominal constant (0.5), ϵ is the energy dissipation, and k is the wave number [*Tennekes and Lumley*, 1972]. The transformation of frequency spectra to wave number spectra is performed by using Taylor's hypothesis by assuming the turbulence is advected past the sensor by the mean velocity (or lowest wave number) with

$$\Phi(k) = \frac{\Phi(f)}{\frac{2\pi}{\tilde{u}}} \tag{12}$$

with

$$k = \frac{2\pi f}{\tilde{u}}. \tag{13}$$

In order for this transformation to be valid, two criteria must be met. First, the mean advection velocity must be greater than the turbulent velocity to satisfy Taylor's frozen flow hypothesis:

$$\tilde{u} \gg u'. \tag{14}$$

Secondly, Lin's criteria [*Lin*, 1953] further specifies that the mean velocity (over a small window of time) must be greater than the change in velocity over the window of calculation. Following *George et al.* [1994], this is interpreted as

$$\tilde{u} \gg \frac{1}{f_{lo}}\frac{\partial\tilde{u}}{\partial t}, \tag{15}$$

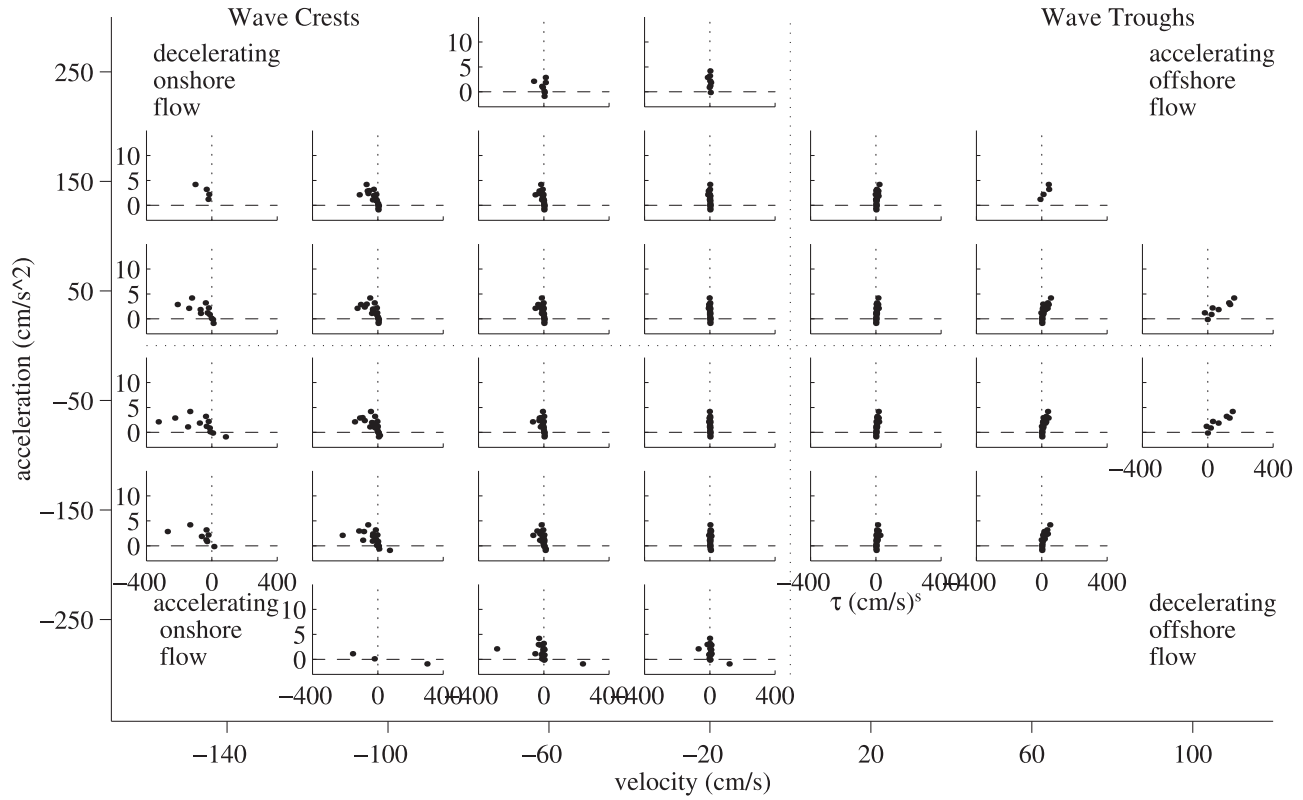

Figure 7. Phase space average distribution of shear stress versus the sensor elevation of the five 256 s WBBL segments. The vertical axis of each independent plot is elevation from the bed, ranging from −2 to 15 cm, and the horizontal axis is stress, ranging from −400 to 400 $(\text{cm s}^{-1})^2$.

where f_{lo} is the lowest frequency over that the spectral calculations were determined. To satisfy this last criteria it was necessary to convert to wave number space only over frequencies greater 8 Hz. A 8 Hz low-frequency cutoff translates to a 9° phase variation over a 5 s wave.

[24] Following the transformation to wave number space, the dissipation rate is found with (11) by fitting a $k^{-\frac{5}{3}}$ line to $\Phi(k)$. Figure 8 shows the PSA of the dissipation estimates that passed the criteria of (14) and (15). Because of occasional spikes in the dissipation rate estimates, a three standard deviation filter was applied to the estimates before computing the phase space averages.

[25] Unlike the turbulent kinetic energy distribution, the dissipation is only slightly enhanced under the wave crests. Only during the extreme wave crests can the dissipation be shown to decrease linearly with increasing sensor elevation, as is predicted in wall bounded shear flow [*Tennekes and Lumley*, 1972]. However, this may be an artifact of the uncertainty in the bed elevation estimate as individual runs (each with an array of 4 hot film anemometers) showed a general tendency for a linear decrease toward the free stream. In general, higher dissipation rates correspond to flatter spectral slopes.

4. Conclusions

[26] Using the first available field turbulence observations of the wave bottom boundary layer it was found that the generation of turbulence is highly intermittent. The intermittent nature of flow was examined by applying homogeneous isotropic turbulence laws over small windows of data. The time varying estimates of turbulent kinetic energy, shear stress, dissipation, and concentration were averaged over the phase space of the free stream wave.

[27] The turbulent kinetic energy generally increases vertically through the wave bottom boundary layer and decreases outside of this layer and is indicative of bottom generated turbulence. The distribution of the turbulent kinetic energy is largest under the wave crest, and decreases over the decelerating flow phase until flow reversal to offshore flow. Slightly enhanced turbulent kinetic energy levels are observed during the latter stages of the onshore accelerating flow. The turbulent kinetic energy levels for the wave trough are less than those under the wave crests for comparable velocity magnitudes. The lower energy levels may be indicative of a sensitivity of turbulence generation to acceleration magnitudes (which are lower under the trough than under the crest) or a suspended sediment induced turbulence dampening. The turbulent kinetic energy observations under the crests compare favorably to those of the three laboratory studies.

[28] The sediment suspension observations were shown to have an intermittent structure and to be biased toward the onshore decelerating phase of the flow. Following suspension under the wave large crests, the plumes were advected back through the sensor array during the accelerating offshore flow. This signature was shown to be coherent with and lag the turbulent kinetic energy observations.

[29] The shear stress was estimated with the orbital velocities by assuming a zero-order eddy viscosity model

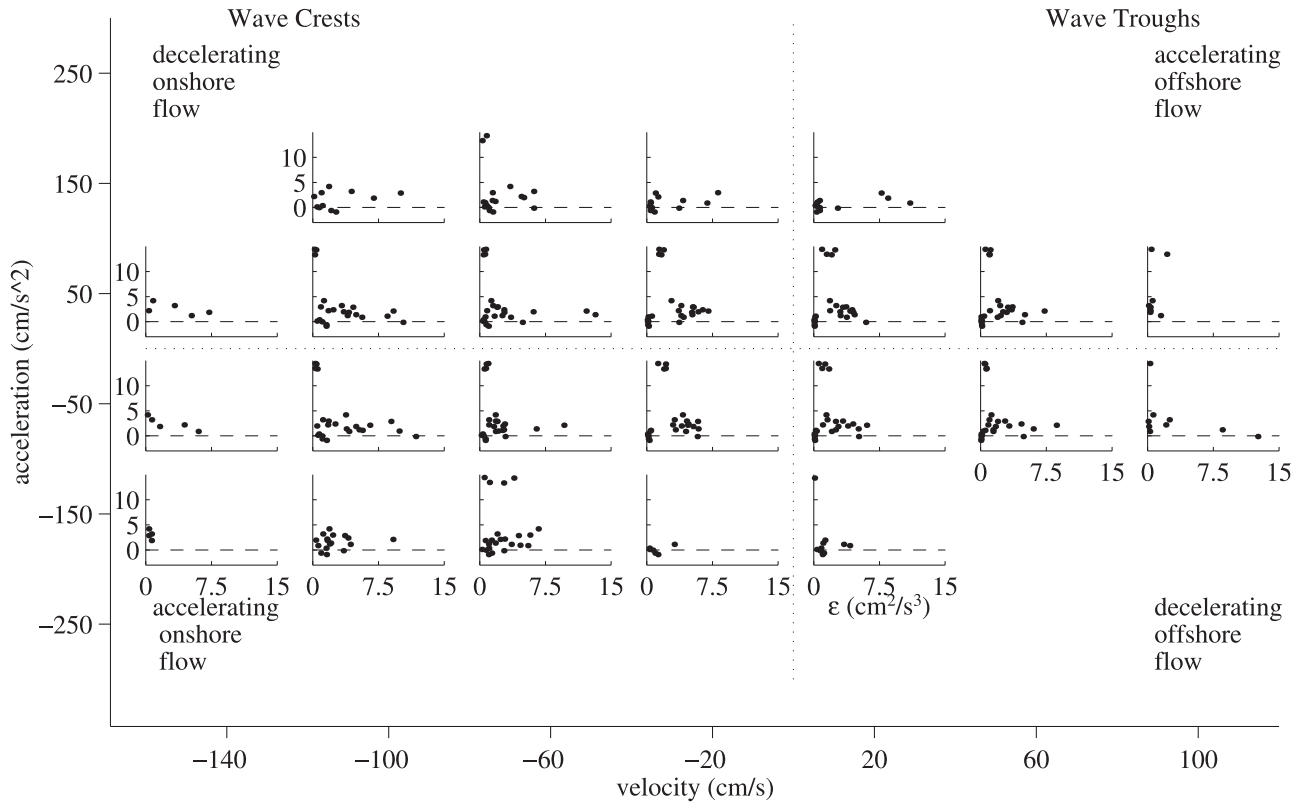

Figure 8. Phase space average distribution of energy dissipation rate versus the sensor elevation of the five 256 s WBBL segments. The vertical axis of each independent plot is elevation from the bed, ranging from −2 to 15 cm, and the horizontal axis is dissipation rate, ranging from −0 to 15 $cm^2\ s^{-3}$.

and shown to be highly sensitive to free stream velocity and less sensitive to free stream acceleration. The peak shear occurs under both the crests and troughs of the wave. For equal free stream velocity magnitudes, the stress under the troughs exceeds the stress under the crests, and is likely attributed to the longer excursion time of the troughs, which allow the boundary layer to develop more than under the shorter duration crests. The intermittent signal of the TKE and suspension was not evident in the shear stress estimates, indicating that simple closure schemes are not appropriate for predicting the suspension of sediment.

[30] Dissipation rate estimates increased with increasing proximity to the bed and were generally an order of magnitude higher than the estimates found outside the wave bottom boundary layer. Not surprisingly, the dissipation rates were several orders of magnitude lower than those observed by *George et al.* [1994] in the active surface breaking region.

[31] **Acknowledgments.** This work was supported by the Office of Naval Research Coastal Geosciences program. We are grateful to Carl Miller and the rest of the FRF field staff for their assistance with instrument deployment and collection of the PUV and accelerometer observations. Early versions of this manuscript benefited from insight provided by Jim Moum.

References

Bagnold, R. A. (1966), An approach to the sediment transport problem from general physics, *U.S. Geol. Surv. Prof. Pap.*, *422-1*, 231–291.

Bailard, J. A. (1981), An energetics total load sediment transport model for a plane sloping beach, *J. Geophys. Res.*, *86*(C11), 938–954.

Beach, R. A., and R. W. Sternberg (1992), Suspended sediment tranpsort in the surf zone: Response to incident wave and longshore surrent interaction, *Mar. Geol.*, *108*, 275–294.

Blackwelder, R. F., and R. E. Kaplan (1976), On the wall structure of the turbulent boundary layer, *J. Fluid Mech.*, *76*, 89–112.

Bowen, A. J. (1980), Simple models of nearshore sedimentation; beach profiles and longshore bars, in *The Coastline of Canada*, edited by S. B. McCan, *Pap. Geol. Surv. Can.*, *80–10*, 1–11.

Conley, D. C., and D. L. Inman (1992), Field observations of the fluid-granular boundary layer under near breaking waves, *J. Geophys. Res.*, *97*(C6), 9631–9643.

Foster, D. L. (1996), Dynamics of the nearshore wave bottom boundary layer, Ph.D. thesis, Oregon State Univ., Corvallis.

Foster, D. L., R. A. Holman, and R. A. Beach (1994), Correlation between sediment suspension events and shear instabilities in the bottom boundary layer of the surf zone, in *Coastal Dynamics '94*, edited by A. S. Arcilla, M. J. F. Stive, and N. C. Kraus, pp. 712–726, Am. Soc. of Civ. Eng., New York.

Foster, D. L., R. A. Beach, and R. A. Holman (2000), Field observations of the wave bottom boundary layer, *J. Geophys. Res.*, *105*(C8), 19,631–19,648.

George, R., R. E. Flick, and R. T. Guza (1994), Observations of turbulence in the surf zone, *J. Geophys. Res.*, *99*(C1), 801–810.

Hanes, D. M. (1988), Intermittent sediment suspension and its implication to sand tracer dispersal in wave-dominated environments, *Mar. Geol.*, *81*, 175–183.

Hino, M., M. Kashiwayanagi, and T. Hara (1983), Experiments on the turbulent statistics and the structure of reciprocating oscillatory flows, *J. Fluid Mech.*, *131*, 363–400.

Huntley, D. A., and D. M. Hanes (1987), Direct measurements of suspended sediment transport, in *Coastal Sediments '87*, edited by N. C. Kraus, pp. 723–737, Am. Soc. of Civ. Eng., New York.

Jaffe, B. E., R. W. Sternberg, and A. H. Sallenger (1984), The role of suspened sediment in shore-normal beahch profile changes, paper presented at 19th International Conference on Coastal Engineering, Am. Soc. of Civ. Eng., Houston, Tex.

Jensen, B. L., B. M. Sumer, and J. Fredsoe (1989), Turbulent oscillatory boundary layers at high reynolds numbers, *J. Fluid Mech.*, *206*, 265–298.

Lin, C. C. (1953), On Taylor's hypothesis and the acceleration terms in the Navier-Stokes equations, *Q. Appl. Math.*, *10*, 295.

Priestley, M. B. (1981), *Spectral Analysis and Time Series*, Elsevier, New York.

Sleath, J. (1987), Turbulent oscillatory flow over rough beds, *J. Fluid Mech.*, *182*, 369–410.

Smyth, C., and A. E. Hay (2003), Near-bed turbulence and bottom friction during Sandy-Duck97, *J. Geophys. Res.*, *108*(C6), 3197, doi:10.1029/2001JC000952.

Tennekes, H., and J. L. Lumley (1972), *A First Course in Turbulence*, MIT Press, Cambridge, Mass.

Thornton, E. B., and R. T. Guza (1983), Transformation of wave height distribution, *J. Geophys. Res.*, *88*(C10), 5925–5938.

R. A. Beach, Consortium for Oceanographic Research and Education, 201 New York Avenue, NW Suite 420, Washington, DC 20005, USA.

D. L. Foster, Department of Civil and Environmental Engineering and Geodetic Science, Ohio State University, Columbus, OH 43210-1275, USA. (foster.316@osu.edu)

R. A. Holman, College of Oceanic and Atmospheric Sciences, Oregon State University, Corvallis, OR 97331, USA.